Field-induced decays in XXZ triangular-lattice antiferromagnets

P. A. Maksimov,[1] M. E. Zhitomirsky,[2] and A. L. Chernyshev[1]

[1]*Department of Physics and Astronomy, University of California, Irvine, California 92697, USA*

[2]*CEA, INAC-PHELIQS, F-38000 Grenoble, France*

(Received 27 July 2016; published 10 October 2016)

We investigate field-induced transformations in the dynamical response of the XXZ model on the triangular lattice that are associated with the anharmonic magnon coupling and decay phenomena. Detailed theoretical predictions are made for $Ba_3CoSb_2O_9$, which provides a close realization of the spin-$\frac{1}{2}$ XXZ model. We demonstrate that dramatic modifications in the magnon spectrum must occur in low out-of-plane fields that are easily achievable for this material. The hallmark of the effect is a coexistence of the clearly distinct well-defined magnon excitations with significantly broadened ones in different regions of the $\mathbf{k}$-ω space. The field-induced decays are generic for this class of models and become more prominent at larger anisotropies and in higher fields.

Introduction. Triangular-lattice antiferromagnets (TLAFs) are central to the field of frustrated magnetism as representatives of one of the basic models epitomizing the effect of spin frustration [1–4]. They have attracted significant experimental and theoretical interests [5–21] as a potential source of spin liquid and of a wide variety of intriguing ordered ground states, see Ref. [22]. Their spectral properties have recently emerged as a subject of intense research that has consistently uncovered broad continuumlike spectral features [6,23,24], which are interpreted as evidence of fractionalized excitations [6,20,25] or of the phenomenon of magnon decay [26–29].

In this Rapid Communication, we outline a theoretical proposal for a dramatic transformation of the spin-excitation spectrum of the XXZ triangular-lattice antiferromagnet in an external out-of-plane field. This consideration pertains in particular to $Ba_3CoSb_2O_9$, one of the close physical realizations of the model that has recently been studied by a variety of experimental techniques [30–34]. The key finding of our Rapid Communication is that a modest out-of-plane field results in a strong damping of the high-energy magnons, affecting a significant part of the $\mathbf{k}$ space. This is different from a similar prediction of the field-induced decays in the square- and honeycomb-lattice AFs where strong spectrum transformations require large fields [35–38]. In the present case, because the staggered chirality of the field-induced umbrella spin structure breaks inversion symmetry, the resultant $\mathbf{k} \leftrightarrow -\mathbf{k}$ asymmetry of the magnon spectrum opens up a channel for decays of the high-energy magnons in a broad vicinity of the K' corners of the Brillouin zone into the two-magnon continuum of the rotonlike magnons at the K points, see Fig. 1 .

We note that the recent neutron-scattering work [23] asserts the existence of an intrinsic broadening in parts of the $Ba_3CoSb_2O_9$ spectrum even in a zero field. Although scatterings due to finite-temperature magnon population or strong effects of disorder in the noncollinear spin structures [39] cannot be ruled out as sources of damping observed in Ref. [23], we would like to point out that the phenomena discussed in this Rapid Communication are substantially more dramatic and should be free from such uncertainties.

Model and spectrum. Owing to frustration and degeneracies of the model, triangular-lattice antiferromagnets in an external

field have a very rich phase diagram [40–45], featuring the hallmark plateau, coplanar, and umbrella states, see Ref. [22] for a recent review. We will focus on the XXZ Hamiltonian with an easy-plane anisotropy whose zero-field ground state is a 120° structure,

$$\hat{\mathcal{H}} = J \sum_{\langle ij \rangle} \left(S_i^x S_j^x + S_i^y S_j^y + \Delta S_i^z S_j^z \right) - H \sum_i S_i^z, \quad (1)$$

where $\langle ij \rangle$ are nearest-neighbor sites of the triangular lattices $J > 0$ and $0 \leqslant \Delta < 1$. In an out-of-plane magnetic field, the so-called umbrella structure is formed, see Fig. 1. In the isotropic limit $\Delta = 1$, the coplanar states are favored instead, but $\Delta < 1$ always stabilizes the semiclassical umbrella state for a range of fields with the $H - \Delta$ region of its stability for $S = 1/2$ sketched in Fig. 2(c) from Ref. [43]. In $Ba_3CoSb_2O_9$, estimates of the anisotropy yield $\Delta \approx 0.9$ [23,33] with an additional stabilization of the umbrellalike state provided by the interplane coupling [34,47]. The LSW treatment of the model (1) within the $1/S$ expansion is standard, see the Supplemental Material [48]. The harmonic magnon energies
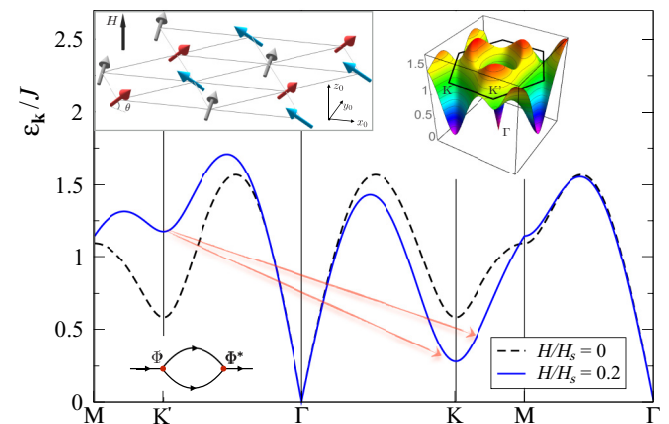

FIG. 1. Linear spin-wave (LSW) energy $\varepsilon_{\mathbf{k}}$ of model (1) for $\Delta = 0.9$, $S = 1/2$ and the fields $H = 0$ and $H = 0.2H_s$. The arrows show schematics of the decay. The insets: umbrella structure in a field, three-dimensional plot of $\varepsilon_{\mathbf{k}}$ for $H = 0.2H_s$, and a decay self-energy diagram.
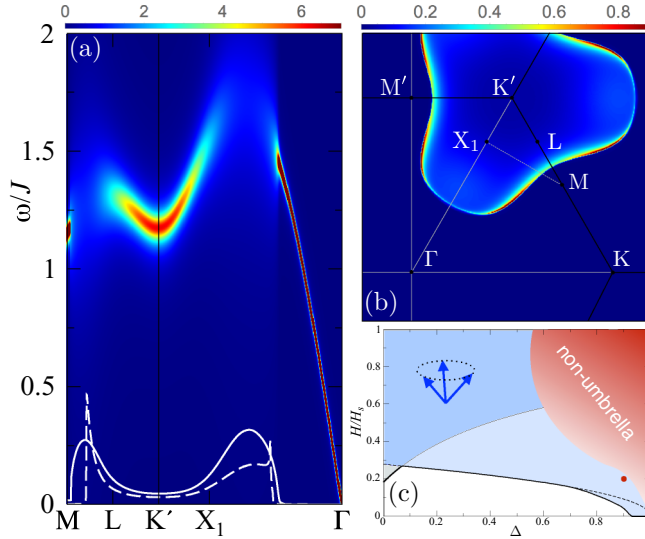
FIG. 2. (a) The intensity plot of the spectral function along the $MK'\Gamma$ path with $\Gamma_\mathbf{k}$ from the self-consistent imaginary Dyson equation (iDE) for $\Delta = 0.9$ and $H = 0.2H_s$. The dashed and solid lines are $\Gamma_\mathbf{k}$ in the Born approximation (2) and the iDE solution. (b) The 2D intensity plot of $\Gamma_\mathbf{k}$ from (2). (c) The $H - \Delta$ diagram of the decay thresholds in the umbrella state. Shaded are the regions where various forms of decay are allowed, see the text. The nonumbrella region for $S = 1/2$ is sketched from Ref. [43]; see Ref. [46]. The dot marks the values of Δ and H used in (a) and (b).

$\varepsilon_\mathbf{k}$ are depicted in Fig. 1 for $S = 1/2$, $\Delta = 0.9$, and $H = 0$ and $H = 0.2H_s$, where $H_s = 6JS(\Delta + 1/2)$ is the saturation field. The chosen representative field of $0.2H_s$ is within the umbrella region of Fig. 2(c), and for $Ba_3CoSb_2O_9$ it corresponds to a modest field of about 6 T [33].

In Fig. 1, one can see the gaps $\propto \sqrt{1 - \Delta}$ at the K and K' points in a zero field. In a finite field, the staggered scalar chirality of the umbrella structure $\mathbf{S}_i \cdot (\mathbf{S}_j \times \mathbf{S}_k)$ induces inversion symmetry breaking. Because of that, magnon energy acquires an asymmetric contribution [49] $\varepsilon_\mathbf{k} \neq \varepsilon_{-\mathbf{k}}$ with the energies at the K (K') points lowered (raised) proportionally to the field. Note that the K and K' points trade their places in the domain with a shifted pattern of the $120°$ order that also corresponds to the flipped staggered chiralities. It is clear that the distorted band structure brings down the energy of a minimum of the two-magnon continuum associated with the low-energy rotonlike magnons at the K points. Given the remaining commensurability of the umbrella state, which retains the $3\mathbf{K} = 0$ property of the $120°$ structure, magnon decays may occur in a proximity of the K' points via a process $\varepsilon_{K'} \Rightarrow \varepsilon_K + \varepsilon_{K(\pm \mathbf{G}_i)}$, where $\mathbf{G}_i$'s are the reciprocal lattice vectors. Although the exact kinematics of such decays is somewhat more complicated, one can simply check where and at what field the on-shell decay conditions $\varepsilon_\mathbf{k} = \varepsilon_\mathbf{q} + \varepsilon_{\mathbf{k}-\mathbf{q}}$ are first met for a given Δ.

This direct verification yields the lower border of the shaded regions in Fig. 2(c), which is a union of three curves. At large anisotropies $\Delta \to 0$, the decay conditions that are fulfilled at the lowest field are the ones associated with the change in the curvature of the Goldstone mode near the Γ point,

the kinematics familiar from the field-induced decays in the square-lattice [35] and honeycomb-lattice AFs [38] as well as ^{4}He [50]. At larger Δ's, the threshold field for decays is precisely determined by the "asymmetry-induced" condition $\varepsilon_{K'} = 2\varepsilon_K$ discussed above, which is given analytically by $H^* = \sqrt{(1 - \Delta)/(13 - \Delta)}$ and is shown by the dashed line in Fig. 2(c). Closer to the isotropic limit $\Delta \gtrsim 0.7$, the decay conditions are first met away from the high-symmetry points; see some discussion of them for the zero-field case and $\Delta > 0.92$ in Ref. [28].

On- (off-) shell decay rate. To get a sense of the quantitative measure of the field-induced broadening effect and of the extent of the affected $\mathbf{k}$ space, we first present the results for the decay rate in the Born approximation,

$$\Gamma_\mathbf{k} = \Gamma_0 \sum_\mathbf{q} |\Phi_{\mathbf{q},\mathbf{k}-\mathbf{q};\mathbf{k}}|^2 \delta(\omega_\mathbf{k} - \omega_\mathbf{q} - \omega_{\mathbf{k}-\mathbf{q}}), \qquad (2)$$

where $\Gamma_0 = 3\pi J/4$ and $\varepsilon_\mathbf{k} = 3JS\omega_\mathbf{k}$. The three-magnon decay vertex $\Phi_{\mathbf{q},\mathbf{k}-\mathbf{q};\mathbf{k}}$ is derived from the anharmonic coupling terms of the $1/S$ expansion of the model (1), see the Supplemental Material [48]. It combines the effects of noncollinearity due to an in-plane $120°$ structure and of the field-induced tilting of spins [26,28,35]. We show $\Gamma_\mathbf{k}$ for a representative $H = 0.2H_s$ and for the same $\Delta = 0.9$ and $S = 1/2$ as above: in Fig. 2(a) along the $MK'\Gamma$ path (dashed line) and in Fig. 2(b) as a two-dimensional (2D) intensity plot.

In addition, we also present the results of the self-consistent solution of the off-shell Dyson equation for $\Gamma_\mathbf{k}$ in which corrections to the magnon energy are ignored but the imaginary part of the the magnon self-energy $\Sigma_\mathbf{k}(\omega)$ due to three-magnon coupling is retained, referred to as the iDE approach: $\Gamma_\mathbf{k} = -\text{Im}\,\Sigma_\mathbf{k}(\varepsilon_\mathbf{k} + i\Gamma_\mathbf{k})$, see Ref. [28]. This method accounts for a damping of the decaying initial-state magnon and regularizes the van Hove singularities associated with the two-magnon continuum that can be seen in the Born results of (2) in Fig. 2(a). The same figure shows the iDE results for $\Gamma_\mathbf{k}$ (solid line) and the corresponding magnon spectral function in a Lorentzian form (intensity plot). We note that the self-consistency schemes that rely on the broadening of the decay products, such as the imaginary self-consistent Born approximation discussed in Refs. [36,51], are not applicable here because our final-state magnons are well defined. Altogether, our consideration suggests that a significant $T = 0$ field-induced broadening of quasiparticle peaks due to magnon decays should appear in a wide vicinity of the K' points in low fields, reaching values of $\Gamma_\mathbf{k} \propto 0.3J$ (cf. $\lesssim 0.1J$ in $Ba_3CoSb_2O_9$ [23]).

Dynamical structure factor. Next, we evaluate the dynamical spin-spin structure factor $\mathcal{S}(\mathbf{q}, \omega)$, the quantity directly observed in the inelastic neutron-scattering experiments. Following Ref. [29] and the Supplemental Material [48], we approximate $\mathcal{S}(\mathbf{q}, \omega)$ as a sum of the diagonal terms of

$$\mathcal{S}^{\alpha_0 \beta_0}(\mathbf{q}, \omega) = \frac{i}{\pi} \text{Im} \int_{-\infty}^{\infty} dt\, e^{i\omega t} \langle T\, S_\mathbf{q}^{\alpha_0}(t) S_{-\mathbf{q}}^{\beta_0}(0) \rangle. \qquad (3)$$

Transforming to the local (rotating) reference frame of the ordered moments and keeping terms that contribute to the
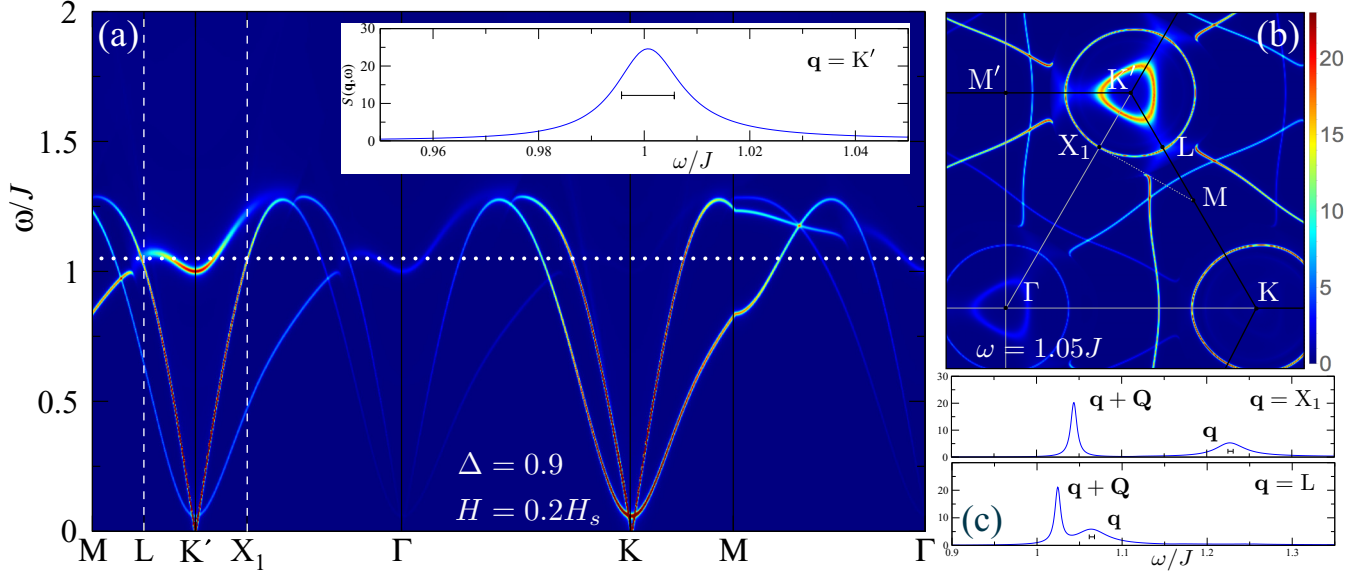
FIG. 3. (a) Intensity plot of $\mathcal{S}(\mathbf{q},\omega)$ along the $MK'\Gamma KM\Gamma$ path. The dotted and dashed lines are constant-energy cuts in (b) and ω cuts in (c). The inset: $\mathcal{S}(\mathbf{q},\omega)$ vs ω at K'. The bars are the artificial width $2\delta = 0.01J$ of the calculation [55]. $S = 1/2$, $\Delta = 0.9$, $H = 0.2H_s$.

leading $1/S$ order [29] yields

$$\mathcal{S}^{x_0 x_0}(\mathbf{q},\omega) = \tfrac{1}{4}\big[\mathcal{S}^{yy}_{\mathbf{q}+} + \mathcal{S}^{yy}_{\mathbf{q}-} + 2i\,\sin\theta\big(\mathcal{S}^{xy}_{\mathbf{q}+} - \mathcal{S}^{xy}_{\mathbf{q}-}\big)$$
$$+ \sin^2\theta\big(\mathcal{S}^{xx}_{\mathbf{q}+} + \mathcal{S}^{xx}_{\mathbf{q}-}\big) + \cos^2\theta\big(\mathcal{S}^{zz}_{\mathbf{q}+} + \mathcal{S}^{zz}_{\mathbf{q}-}\big)\big],$$

$$\mathcal{S}^{z_0 z_0}(\mathbf{q},\omega) = \cos^2\theta\,\mathcal{S}^{xx}_{\mathbf{q}} + \sin^2\theta\,\mathcal{S}^{zz}_{\mathbf{q}}, \qquad (4)$$

and $\mathcal{S}^{y_0 y_0}(\mathbf{q},\omega) = \mathcal{S}^{x_0 x_0}(\mathbf{q},\omega)$. Here we used the antisymmetric nature of the xy contribution $\mathcal{S}^{xy}_{\mathbf{q}} = -\mathcal{S}^{yx}_{\mathbf{q}}$ and introduced shorthand notations for $\mathcal{S}^{\alpha\beta}_{\mathbf{q}} \equiv \mathcal{S}^{\alpha\beta}(\mathbf{q},\omega)$ and shifted momenta $\mathbf{q}\pm \equiv \mathbf{q}\pm\mathbf{K}$ with θ being the out-of-plane canting angle of spins. In the local reference frame, $\mathcal{S}^{zz}_{\mathbf{q}}$ components of the dynamical structure factor are "longitudinal," i.e., are due to the two-magnon continuum, having no sharp quasiparticle features [29]. The rest of Eq. (4) is "transverse," i.e., is related to the single-magnon spectral function $\mathcal{S}^{x(y)x(y)}_{\mathbf{q}} \propto A(\mathbf{q},\omega)$ with different kinematic $\mathbf{q}$-dependent form factors, where $A(\mathbf{q},\omega) = -(1/\pi)\text{Im}\,G(\mathbf{q},\omega)$ and the diagonal magnon Green's function is $G(\mathbf{q},\omega) = [\omega - \varepsilon_{\mathbf{q}} - \Sigma_{\mathbf{q}}(\omega) + i\delta]^{-1}$. Thus, the dynamical structure factor of the XXZ TLAF in a field should feature three overlapping single-magnon spectral functions $A(\mathbf{q},\omega)$ and $A(\mathbf{q}\pm\mathbf{K},\omega)$ with different weights according to (4) and the Supplemental Material [48]; see also Ref. [52].

In our consideration, we include all contributions to the one-loop magnon self-energy $\Sigma_{\mathbf{q}}(\omega)$ of the $1/S$ order of the nonlinear spin-wave theory [26]. Namely, there are two more terms in addition to the decay diagram: the source diagram and the Hartree-Fock correction; the latter composed of the contributions from the four-magnon interactions (quartic terms) and from the quantum corrections to the out-of-plane canting angle of spins, see the Supplemental Material [48] for technical details,

$$\Sigma_{\mathbf{q}}(\omega) = \Sigma^{\text{HF}}_{\mathbf{q}} + \Sigma^d_{\mathbf{q}}(\omega) + \Sigma^s_{\mathbf{q}}(\omega). \qquad (5)$$

Having included all one-loop contributions also allows us to consistently take into account the ω dependence of the magnon

spectral function. Below we demonstrate that anharmonic interactions lead to the broadening of magnon quasiparticle peaks, redistribution of spectral weight, and other dramatic changes in the spectrum.

In Fig. 3, we present our results for the dynamical structure factor $\mathcal{S}(\mathbf{q},\omega)$ in (4) of the model (1) for $S = 1/2$, $\Delta = 0.9$, and $H = 0.2H_s$. First, there is a strong downward bandwidth renormalization by about 30% compared to the LSW results in Fig. 1, which is characteristic of the TLAFs [18,27,28]. The most important result is a significant broadening of the magnon spectra for an extensive range of momenta, accompanied by well-pronounced termination points with distinctive bending of spectral lines [54] and other non-Lorentzian features that are associated with crossings of the two-magnon continuum. The broadening can be seen in a wide proximity of the K' points of the Brillouin zone as well as in the equivalent regions of the "$\pm\mathbf{K}$-shifted" components of the structure factor. Despite the strong renormalization of the spectrum, the extent of the affected $\mathbf{q}$ region is about the same as in the on-shell consideration in Fig. 2.

The inset of Fig. 3(a) shows $\mathcal{S}(\mathbf{q},\omega)$ vs ω at a representative K' point that exhibits a modest broadening compared with the artificial width (2δ) of the calculation. The ω cuts at the X_1 and L points near the boundaries of the decay region in Fig. 3(c) show much heavier damping in one of the components of $\mathcal{S}(\mathbf{q},\omega)$, which coexists with the well-defined spectral peak from the shifted component. The enhancement of magnon decays near the edge of the decay region also correlates well with the on-shell results in Fig. 2 and points to the van Hove singularities of the two-magnon continuum as a culprit. The 2D intensity map of the constant-energy cut of $\mathcal{S}(\mathbf{q},\omega)$ at $\omega = 1.05J$ is shown in Fig. 3(b) where one can see multiple signatures of the broadening, spectral weight redistribution around K', and termination points.

Larger anisotropy. We complement our consideration of the model (1) by demonstrating the effects of the magnetic field on the magnon spectrum for the TLAFs with large easy-plane
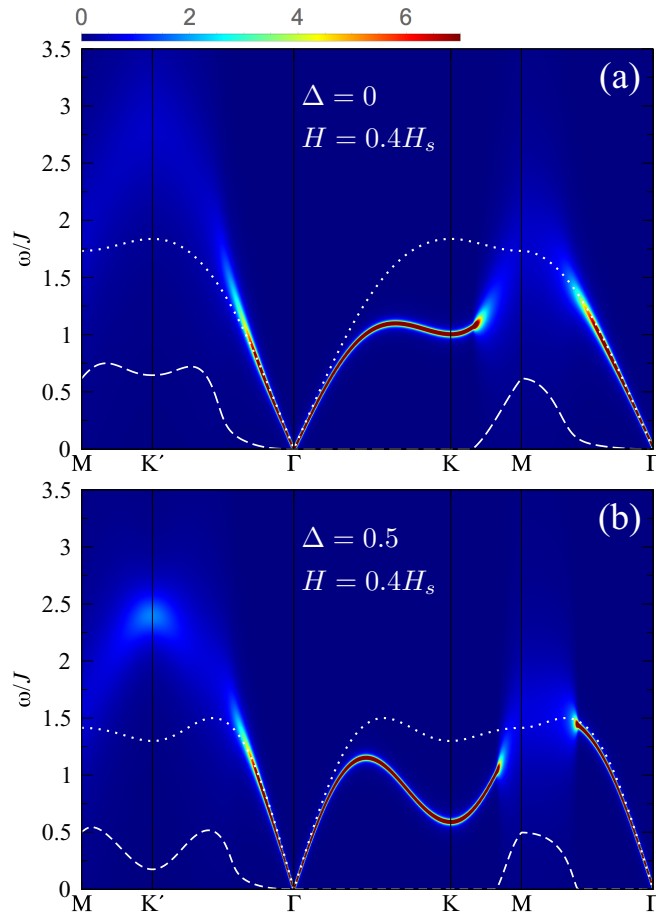
FIG. 4. Intensity plots of the spectral function with the iDE $\Gamma_{\mathbf{k}}$ (dashed lines) for $S = 1/2$, $H = 0.4H_s$, and $\Delta = 0$ in (a) and $\Delta = 0.5$ in (b). The dotted lines are the LSW spectra for $H = 0$.

and the second shows strong spectrum renormalization that avoids decays for $H \lesssim 0.5H_s$. Since the reason for this discrepancy is the lack of self-consistency, we resort to the (partially) self-consistent iDE approach described above. In Fig. 4, we show its results for the magnon spectral function with the Lorentzian broadening $\Gamma_{\mathbf{k}}$ for $\Delta = 0$, $\Delta = 0.5$, and $H = 0.4H_s$. What is remarkable is not only a persistent pattern of a wide $\mathbf{k}$ region of the strongly overdamped high-energy magnons [cf., Fig. 2(a)], but also the magnitudes of their broadening, which reach the values of almost a half of the magnon bandwidth even after a self-consistent regularization.

Conclusions. We have provided a detailed analysis of the field-induced dynamical response of the XXZ model on the triangular lattice within the umbrella phase. We have demonstrated a ubiquitous presence of significant damping of the high-energy magnons already in moderate fields $H \gtrsim 0.2H_s$. Other characteristic features, such as significant spectral weight redistribution and termination points that separate well-defined excitations from the ones that are overdamped, are also expected to occur. The key physical ingredients of this dramatic spectral transformation are a strong spin noncollinearity, which is retained by the umbrella state and is essential for the anharmonic magnon coupling and decays, and the tilted $\mathbf{k} \leftrightarrow -\mathbf{k}$ asymmetric magnon band structure, owing its origin to the staggered chirality of the umbrella state that breaks the inversion symmetry. Our consideration pertains in particular to $Ba_3CoSb_2O_9$, which is currently a prime candidate for observing aforementioned properties in reasonably small fields reachable in experimental setups. Our Rapid Communication should be a qualitative and quantitative guidance for observations of the dynamical structure factor in the inelastic neutron-scattering experiments in this and other related systems.

anisotropy. In the strongly anisotropic limit $\Delta = 0$, the nonlinear anharmonic coupling of magnons is known to result in a very strong spectrum renormalization (about 50%) but with no decays kinematically allowed [28]. For $S = 1/2$ and small enough Δ, the Born approximation and the $1/S$ one-loop ω-dependent self-energy approach are somewhat inconsistent in that the first produces unphysically large $\Gamma_{\mathbf{k}}$ for $H \gtrsim 0.3H_s$

[1] G. H. Wannier, Phys. Rev. **79**, 357 (1950).

[2] P. W. Anderson, Mater. Res. Bull. **8**, 153 (1973); P. Fazekas and P. W. Anderson, Philos. Mag. **30**, 423 (1974).

[3] D. A. Huse and V. Elser, Phys. Rev. Lett. **60**, 2531 (1988).

[4] D. H. Lee, J. D. Joannopoulos, J. W. Negele, and D. P. Landau, Phys. Rev. Lett. **52**, 433 (1984).

[5] M. F. Collins and O. A. Petrenko, Can. J. Phys. **75**, 605 (1997).

[6] R. Coldea, D. A. Tennant, A. M. Tsvelik, and Z. Tylczynski, Phys. Rev. Lett. **86**, 1335 (2001); R. Coldea, D. A. Tennant, K. Habicht, P. Smeibidl, C. Wolters, and Z. Tylczynski, *ibid.* **88**, 137203 (2002).

[7] L. E. Svistov, A. I. Smirnov, L. A. Prozorova, O. A. Petrenko, L. N. Demianets, and A. Ya. Shapiro, Phys. Rev. B **67**, 094434 (2003).

[8] S. Nakatsuji, Y. Nambu, H. Tonomura, O. Sakai, S. Jonas, C. Broholm, H. Tsunetsugu, Y. Qiu, and Y. Maeno, Science **309**, 1697 (2005).

[9] A. Olariu, P. Mendels, F. Bert, B. G. Ueland, P. Schiffer, R. F. Berger, and R. J. Cava, Phys. Rev. Lett. **97**, 167203 (2006).

[10] T. Oguchi, J. Phys. Soc. Jpn. Suppl. **52**, 183 (1983).

[11] Th. Jolicoeur and J. C. Le Guillou, Phys. Rev. B **40**, 2727 (1989).

[12] S. J. Miyake, J. Phys. Soc. Jpn. **61**, 983 (1992).

[13] A. V. Chubukov, S. Sachdev, and T. Senthil, J. Phys.: Condens. Matter **6**, 8891 (1994).

[14] P. W. Leung and K. J. Runge, Phys. Rev. B **47**, 5861 (1993).

[15] B. Bernu, P. Lecheminant, C. Lhuillier, and L. Pierre, Phys. Rev. B **50**, 10048 (1994).

[16] L. Capriotti, A. E. Trumper, and S. Sorella, Phys. Rev. Lett. **82**, 3899 (1999).

[17] Z. Weihong, J. Oitmaa, and C. J. Hamer, Phys. Rev. B **44**, 11869 (1991).

[18] W. Zheng, J. O. Fjærestad, R. R. P. Singh, R. H. McKenzie, and R. Coldea, Phys. Rev. B **74**, 224420 (2006).

[19] S. R. White and A. L. Chernyshev, Phys. Rev. Lett. **99**, 127004 (2007).

[20] O. A. Starykh, H. Katsura, and L. Balents, Phys. Rev. B **82**, 014421 (2010).

[21] Z. Zhu and S. R. White, Phys. Rev. B **92**, 041105 (2015).

[22] O. A. Starykh, Rep. Prog. Phys. **78**, 052502 (2015).

[23] J. Ma, Y. Kamiya, T. Hong, H. B. Cao, G. Ehlers, W. Tian, C. D. Batista, Z. L. Dun, H. D. Zhou, and M. Matsuda, Phys. Rev. Lett. **116**, 087201 (2016).

[24] J. Oh, M. Duc Le, J. Jeong, J.-h. Lee, H. Woo, W.-Y. Song, T. G. Perring, W. J. L. Buyers, S.-W. Cheong, and J.-G. Park, Phys. Rev. Lett. **111**, 257202 (2013).

[25] E. A. Ghioldi, A. Mezio, L. O. Manuel, R. R. P. Singh, J. Oitmaa, and A. E. Trumper, Phys. Rev. B **91**, 134423 (2015).

[26] M. E. Zhitomirsky and A. L. Chernyshev, Rev. Mod. Phys. **85**, 219 (2013).

[27] O. A. Starykh, A. V. Chubukov, and A. G. Abanov, Phys. Rev. B **74**, 180403 (2006).

[28] A. L. Chernyshev and M. E. Zhitomirsky, Phys. Rev. Lett. **97**, 207202 (2006); Phys. Rev. B **79**, 144416 (2009).

[29] M. Mourigal, W. T. Fuhrman, A. L. Chernyshev, and M. E. Zhitomirsky, Phys. Rev. B **88**, 094407 (2013).

[30] Y. Doi, Y. Hinatsu, and K. Ohoyama, J. Phys.: Condens. Matter **16**, 8923 (2004).

[31] Y. Shirata, H. Tanaka, A. Matsuo, and K. Kindo, Phys. Rev. Lett. **108**, 057205 (2012).

[32] H. D. Zhou, C. Xu, A. M. Hallas, H. J. Silverstein, C. R. Wiebe, I. Umegaki, J. Q. Yan, T. P. Murphy, J.-H. Park, Y. Qiu, J. R. D. Copley, J. S. Gardner, and Y. Takano, Phys. Rev. Lett. **109**, 267206 (2012).

[33] T. Susuki, N. Kurita, T. Tanaka, H. Nojiri, A. Matsuo, K. Kindo, and H. Tanaka, Phys. Rev. Lett. **110**, 267201 (2013).

[34] G. Koutroulakis, T. Zhou, Y. Kamiya, J. D. Thompson, H. D. Zhou, C. D. Batista, and S. E. Brown, Phys. Rev. B **91**, 024410 (2015).

[35] M. E. Zhitomirsky and A. L. Chernyshev, Phys. Rev. Lett. **82**, 4536 (1999).

[36] M. Mourigal, M. E. Zhitomirsky, and A. L. Chernyshev, Phys. Rev. B **82**, 144402 (2010).

[37] W. T. Fuhrman, M. Mourigal, M. E. Zhitomirsky, and A. L. Chernyshev, Phys. Rev. B **85**, 184405 (2012).

[38] P. A. Maksimov and A. L. Chernyshev, Phys. Rev. B **93**, 014418 (2016).

[39] W. Brenig and A. L. Chernyshev, Phys. Rev. Lett. **110**, 157203 (2013).

[40] H. Kawamura and S. Miyashita, J. Phys. Soc. Jpn. **54**, 4530 (1985).

[41] S. E. Korshunov, J. Phys. C **19**, 5927 (1986).

[42] A. V. Chubukov and D. I. Golosov, J. Phys.: Condens. Matter **3**, 69 (1991).

[43] D. Yamamoto, G. Marmorini, and I. Danshita, Phys. Rev. Lett. **112**, 127203 (2014).

[44] G. Marmorini, D. Yamamoto, and I. Danshita, Phys. Rev. B **93**, 224402 (2016).

[45] D. Sellmann, X.-F. Zhang, and S. Eggert, Phys. Rev. B **91**, 081104 (2015).

[46] The phase diagrams in Refs. [43,45] are slightly different.

[47] R. S. Gekht and I. N. Bondarenko, J. Exp. Theor. Phys. **84**, 345 (1997).

[48] See Supplemental Material at http://link.aps.org/supplemental/10.1103/PhysRevB.94.140407 for details on the nonlinear spin-wave theory.

[49] M. E. Zhitomirsky and I. A. Zaliznyak, Phys. Rev. B **53**, 3428 (1996).

[50] L. P. Pitaevskii, Zh. Eksp. Teor. Fiz. **36**, 1168 (1959) [Sov. Phys. JETP **9**, 830 (1959)].

[51] T. J. Sluckin and R. M. Bowley, J. Phys. C **7**, 1779 (1974).

[52] In experimental systems, one expects domains with opposite patterns of staggered chirality to form. In that case, the dynamical structure factor $\mathcal{S}(\mathbf{q},\omega)$ is a superposition of Fig. 3 and its mirror image. The single-domain chiral order can be produced, e.g., by using the magnetoelectric effect [53].

[53] M. Mourigal, M. Enderle, R. K. Kremer, J. M. Law, and B. Fåk, Phys. Rev. B **83**, 100409 (2011).

[54] K. W. Plumb, K. Hwang, Y. Qiu, L. W. Harriger, G. E. Granroth, A. I. Kolesnikov, G. J. Shu, F. C. Chou, C. Rüegg, Y. B. Kim, and Y.-J. Kim, Nat. Phys. **12**, 224 (2016).

[55] Calculations of the self-energy $\Sigma_{\mathbf{k}}(\omega)$ were performed with a smaller artificial broadening $\delta' = 0.0005J$.